

Evolution of the Fermi surface of arsenic through the rhombohedral to simple-cubic phase transition: a Wannier interpolation study—supplementary information

Patricia K. Silas,¹ Peter D. Haynes,² and Jonathan R. Yates³

¹*Theory of Condensed Matter, Cavendish Laboratory, University of Cambridge, JJ Thomson Avenue, Cambridge CB3 0HE, United Kingdom*

²*Departments of Materials and Physics, Imperial College London, Exhibition Road, London SW7 2AZ, United Kingdom*

³*Department of Materials, University of Oxford, Parks Road, Oxford OX1 3PH, United Kingdom*
(Dated: September 16, 2013)

We review the Brillouin zone (BZ) corresponding to the two-atom primitive cell of rhombohedral (A7) arsenic, defining explicitly the special \mathbf{k} -points involved. This is followed by a discussion concerning the choice of the number of Wannier functions to construct in order to set up an “exact tight-binding” model at each given pressure from which Wannier interpolations can be performed. We elaborate on the features of the electron and hole Fermi surfaces of A7 arsenic at 0 GPa. We investigate the case of simple-cubic (sc) arsenic at 35 GPa using the one-atom primitive cell in order to inspect the “unfolded” Fermi surfaces, and to compare with the folded ones resulting from the use of the two-atom unit cell. We present the results of our studies of arsenic at pressures beyond which it is no longer in the sc phase, where once again the two-atom unit cell is employed. Finally, we elaborate on our studies of the density of states (DOS) of arsenic as it undergoes the A7 \rightarrow sc (space groups $R\bar{3}m \rightarrow Pm\bar{3}m$) phase transition, and present DOS for A7, sc and body-centered-cubic (bcc) arsenic (space group $Im\bar{3}m$). These DOS are contrasted against the band structures from which they originate.

SI. THE RHOMBOHEDRAL BRILLOUIN ZONE

The real-space primitive cell of A7 arsenic contains two atoms and is described by three lattice parameters: the length of the lattice vectors, a , the angle α between each pair of lattice vectors, and the atomic positional parameter z , where $z < 1/4$, which determines the fractional positions of the two atoms along the cell’s body diagonal. The BZ of the primitive rhombohedral structure—it is the same for each of the group-V semimetals: arsenic, antimony and bismuth—is presented in Fig. S1.³² This figure was taken from Ref. 1, though it was originally published by M. H. Cohen in 1961.² Cohen, Falicov and Golin³ showed that much of the band structure of the group-V semimetals can be explained directly from their crystal structure.

The parameter ϵ as defined in Ref. 4 describes the shear that distorts the A7 structure from the sc structure. It is related to the rhombohedral angle α thus:

$$\epsilon = \frac{\left[1 - (1 + \cos \alpha - 2 \cos^2 \alpha)^{1/2}\right]}{\cos \alpha}. \quad (1)$$

The structure of A7 arsenic can be pictured by imagining the interpenetration of two face-centered-cubic lattices (each one contributing an atom to the two-atom A7 primitive cell) offset from each other such that $z < 1/4$ and to which a shear has been applied in the $[111]$ direction (along the trigonal axis), such that $\alpha < 60^\circ$. When $\alpha = 60^\circ$, $\epsilon = 0$ and there is no shear—when both lattice parameters reach their high-symmetry values, $\alpha = 60^\circ$ and $z = 1/4$, the structure becomes simple cubic.

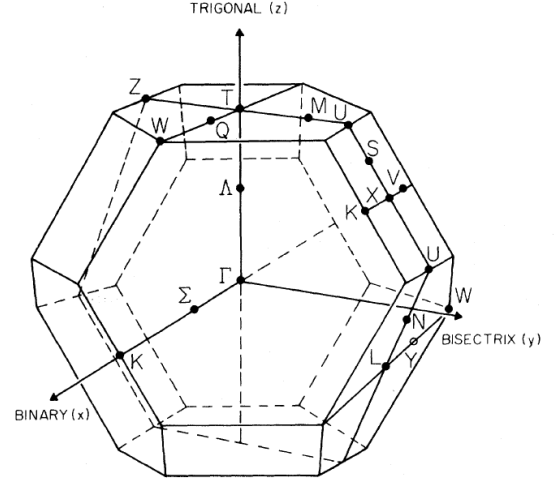


FIG. S1: The BZ of the primitive rhombohedral (A7) structure, labeled with points and lines of symmetry^{2,4} and with the mutually orthogonal binary (x), bisectrix (y) and trigonal (z) axes. This figure is taken from Ref. 1.

The special \mathbf{k} -points of the rhombohedral BZ indicated in Fig. S1 have been written out explicitly by Falicov and Golin,⁴ who follow Cohen’s notation for points and lines of symmetry.² These points of symmetry are expressed in fractional coordinates (with respect to the reciprocal lattice vectors). Examples of each of these points are:

$$\Gamma = [0, 0, 0], \quad (2)$$

$$X = \left[0, \frac{1}{2}, \frac{1}{2}\right], \quad (3)$$

$$L = \left[0, \frac{1}{2}, 0\right], \quad (4)$$

$$T = \left[\frac{1}{2}, \frac{1}{2}, \frac{1}{2}\right], \quad (5)$$

$$W = \left[\gamma, 1 - \gamma, \frac{1}{2}\right], \quad (6)$$

$$U = \left[\frac{1}{2}\gamma + \frac{1}{4}, 1 - \gamma, \frac{1}{2}\gamma + \frac{1}{4}\right], \quad (7)$$

$$K = \left[0, \frac{3}{4} - \frac{1}{2}\gamma, \frac{1}{2}\gamma + \frac{1}{4}\right], \quad (8)$$

where⁴

$$\gamma = \frac{(1 + \frac{1}{2}\epsilon^2)}{(2 + \epsilon)^2}. \quad (9)$$

Multiplicities and symmetry elements of these special \mathbf{k} -points can be found in Cohen.² Other group theoretical considerations can be found in Falicov and Golin.⁴

Note that the three special points W, U and K depend on γ , and thus on the rhombohedral angle α of the real-space primitive cell—their coordinates will therefore change as the pressure is increased. When $\alpha = 60^\circ$, $\epsilon = 0$ and $\gamma = \frac{1}{4}$. Thus in the two-atom representation of sc arsenic:

$$W_{sc} = \left[\frac{1}{4}, \frac{3}{4}, \frac{1}{2}\right], \quad (10)$$

$$U_{sc} = \left[\frac{3}{8}, \frac{3}{4}, \frac{3}{8}\right], \quad (11)$$

$$K_{sc} = \left[0, \frac{5}{8}, \frac{3}{8}\right]. \quad (12)$$

As $\alpha \rightarrow 90^\circ$, $\epsilon \rightarrow -0.5$ and $\gamma = \frac{1}{2}$. Thus in the two-atom representation of bcc arsenic, the points W and U merge with T, and the point K merges with X:

$$W_{bcc} = U_{bcc} = T = \left[\frac{1}{2}, \frac{1}{2}, \frac{1}{2}\right], \quad (13)$$

$$K_{bcc} = X = \left[0, \frac{1}{2}, \frac{1}{2}\right]. \quad (14)$$

The convention is to label the three mutually orthogonal axes making up the coordinate system of the A7 BZ as follows. Referring again to Fig. S1, the binary axis is labeled the x -axis and contains the segment ΓK —it is parallel to the TW line. The bisectrix axis is labeled as the y -axis—it is parallel to the TU line but passes through Γ . The trigonal (z) axis passes through the segment ΓT . The trigonal and bisectrix axes define a mirror plane.

Angles measured in the BZ are reported according to a convention that is discussed in Refs. 5–8 and in Ref. 1. In the trigonal-bisectrix (mirror) plane, or some parallel

plane, angles are measured with respect to the vertical (the trigonal axis, ΓT , or some parallel line). Positive rotations are in the sense from ΓT to ΓX in the first quadrant of the coordinate system. Our calculations of the unit cell of arsenic yield the following angles for the special points in the mirror plane: ΓT is at 0° , ΓX is at $+58.4^\circ$, ΓU is at $+41.3^\circ$ and ΓL is at -72.9° . These values are for the configuration resulting from a geometry optimization of A7 arsenic at 0 GPa (and 0 K) using the Perdew-Burke-Ernzerhof generalized gradient approximation⁹ (abbreviated in this work as GGA-PBE) for the exchange-correlation functional. The details of these calculations can be found in Ref. 10

We will make some brief comparisons here and there between the two-atom and one-atom (primitive) cells of sc arsenic. The BZ for the one-atom primitive sc structure can be found for example in Ref. 3 or more recently in Ref. 11. Examples of the special points of this BZ are $\Gamma = [0, 0, 0]$, $R = [\frac{1}{2}, \frac{1}{2}, \frac{1}{2}]$, $M = [\frac{1}{2}, \frac{1}{2}, 0]$ and $X = [\frac{1}{2}, 0, 0]$. The BZ of the primitive sc structure is the “unfolded” version of the BZ of the two-atom unit cell in the sc configuration. In the two-atom BZ, the point R folds onto the point Γ , and the point M folds onto the point X.³

SII. CHOICE OF THE NUMBER OF WANNIER FUNCTIONS TO CONSTRUCT

Initially, we began our studies using four Wannier functions per atom of the unit cell—the initial guesses for these were the hybrid sp^3 orbitals.¹² However as is demonstrated in Fig. S2, in which the Wannier-interpolated bands (in green) have been obtained using four Wannier functions per atom of the unit cell, this choice turns out not to be well suited to studying arsenic at higher pressures. This is evidenced by the inability of the four Wannier functions to capture the states of the (red) *ab initio* band structure which can be seen to be descending (one of which in heavy black) toward the Fermi level with increasing pressure. In addition, in order for the band structure to be faithfully reproduced using only four Wannier functions at the higher pressures, we would be obliged to keep the “inner window” quite close to the Fermi level (see especially the bottom panel of Fig. S2, the band structure of arsenic at 200 GPa), yet we would like ideally to be able to place it a few eV above the Fermi level. (The inner window is the energy window within which the *ab initio* band structure is required to be preserved as per the disentanglement method of Souza, Marzari and Vanderbilt.¹³)

We choose therefore to address both points by working with nine Wannier functions per atom of the unit cell over the entire range of pressures studied. The trial functions used for the initial guesses of the nine Wannier functions are the six sp^3d^2 hybrid orbitals in addition to the d_{xy} , d_{yz} and d_{xz} orbitals,¹² all atom-centered, and this turns out to be entirely satisfactory.

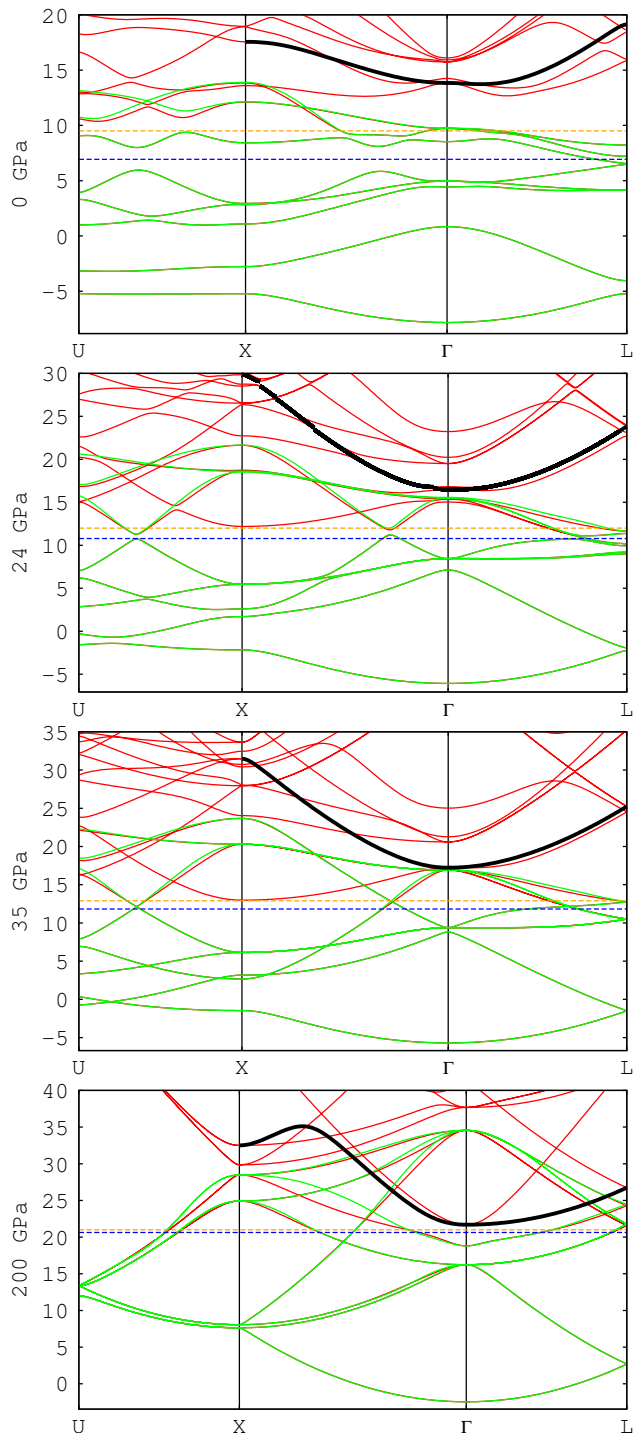


FIG. S2: Band structures of arsenic at 0, 24, 35 and 200 GPa (energy in eV). The Wannier-interpolated bands (in green) have been obtained using four Wannier functions per atom of the unit cell. The dotted blue line is the Fermi level and the dotted pink line indicates the top of the “inner window”. Arsenic is in the A7 phase at 0 and 24 GPa, in the sc phase at 35 GPa, and in the bcc phase at 200 GPa. Using four Wannier functions is not suitable for arsenic at higher pressures. As the pressure increases certain *ab initio* bands can be seen to be descending toward the Fermi level. One of these states is outlined in black—this state is not captured by the four sp^3 orbitals used as the initial guess for the Wannier functions.

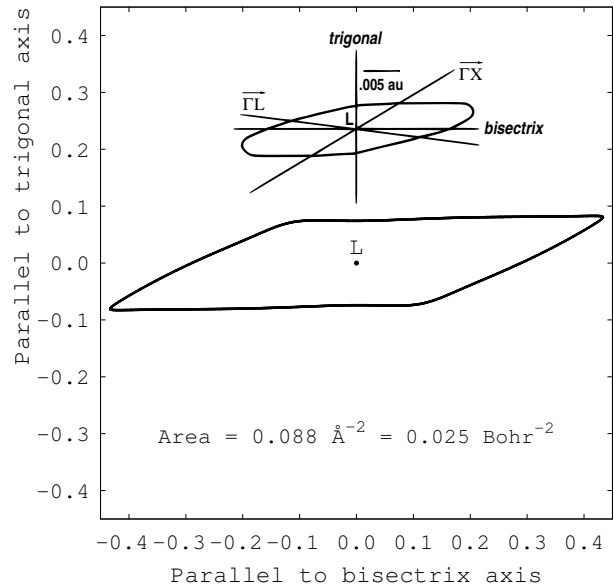


FIG. S3: Electron pocket: trigonal-bisectrix plane through L. This figure and the resulting area have been obtained using a Fermi energy recomputed from the Wannier-interpolated DOS of A7 arsenic at 0 GPa. All distances are in \AA^{-1} . This contour can be located in the top panel of the left-hand column of Fig. 6. The inset is the analogous cross section as calculated by Lin and Falicov.¹⁴

SIII. FURTHER DETAILS OF THE ELECTRON AND HOLE FERMI SURFACES

A. Features of the Electron Fermi Surface

The electron Fermi surface of arsenic at 0 GPa is composed of three ellipsoid-like pockets centered at the three equivalent L points of the BZ. The intersection of the trigonal-bisectrix plane (the mirror plane) with an electron pocket at L results in the Fermi contour illustrated in Fig. S3. We have included as an inset of this figure the analogous cross section obtained by Lin and Falicov in 1966.¹⁴

Before we proceed, it is important to note that the Lin and Falicov calculations were based on experimental data (from de Haas-van Alphen experiments performed at temperatures between 1.2 and 4.2 K) available at the time—most of it available to them by private communication,¹⁴ values which were later somewhat altered upon their publication.⁷ Lin and Falicov fixed the Fermi energies of the electron and hole Fermi surfaces so as to fit the data available for certain features contained therein. In the case of the electron Fermi surface, the Fermi energy was adjusted to fit an area corresponding to the minimum area observed for magnetic fields in the trigonal-bisectrix plane.^{7,14} In the case of the hole Fermi surface, the Fermi energy was adjusted to fit the area reported by Priestly, et al.⁷ to correspond to a cross section of one of the long

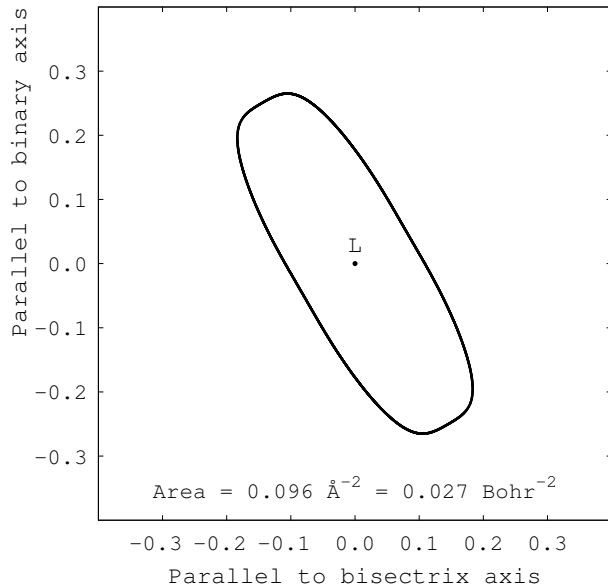


FIG. S4: Electron pocket: binary-bisectrix plane through L. This figure and the resulting area have been obtained using a Fermi energy recomputed from the Wannier-interpolated DOS of A7 arsenic at 0 GPa. All distances are in \AA^{-1} . This contour can be located in the top panel of the middle column of Fig. 6.

thin “necks”. Thus the calculations of Lin and Falicov have been adjusted to fit some prevalent experimental data. Nevertheless it is still edifying to compare our results with theirs.

Returning thus to Fig. S3, we see that the contour of our electron pocket in the trigonal-bisectrix plane is quite a bit sharper than that of Lin and Falicov. The area of this cross section, 0.088\AA^{-2} , is approximately 20% larger than that obtained from those early experiments, and it is approximately 55% larger than that of Lin and Falicov. The long axis of the electron pocket makes an angle of 10.6° with the horizontal—this is similar to what was found both theoretically¹⁴ and experimentally.^{1,7}

Careful inspection of Fig. S3 leads us to believe that this cross section is somewhat “S-shaped”. This observation is corroborated experimentally for arsenic by Priestley, *et al.*⁷ and by Cooper and Lawson,¹ who performed cyclotron resonance experiments for arsenic at 1.15 K. This “S-shape” has also been calculated by Falicov and Lin as being the case for the analogous cross section in antimony.⁵

The intersection of the binary-bisectrix plane with an electron pocket at L results in the cross section of area 0.096\AA^{-2} presented in Fig. S4, and the intersection of the trigonal-binary plane with an electron pocket at L yields the contour of area 0.026\AA^{-2} displayed in Fig. S5—this cross section corresponds to that obtained by slicing the electron pocket of Fig. S3 in the vertical direction at L. These results, as well as those that follow for the hole Fermi surface of arsenic at 0 GPa, are summarized in Table I, along with data resulting from theory and

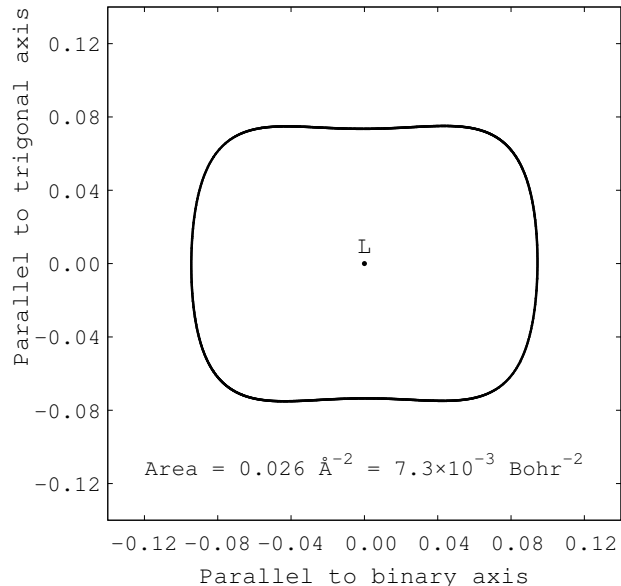


FIG. S5: Electron pocket: trigonal-binary plane through L. This figure and the resulting area have been obtained using a Fermi energy recomputed from the Wannier-interpolated DOS of A7 arsenic at 0 GPa. All distances are in \AA^{-1} .

experiment available in the literature.

B. Features of the Hole Fermi Surface

The hole Fermi surface of arsenic at 0 GPa is an object centered at T composed of six lobe-like pockets (three up, three down) connected by long thin cylinders or “necks”. The intersection of the trigonal-bisectrix plane (the mirror plane) with one of the lobe-like hole pockets results in the Fermi contour displayed in Fig. S6. Once again, we include as an inset of this figure the analogous cross section obtained by Lin and Falicov in 1966.¹⁴ Again, our respective contours are similar, though slightly different toward the extremities. The area of our cross section is 0.027\AA^{-2} , which is about twice as large as in Ref. 7 (experiment), approximately 1% larger than in Ref. 1 (experiment), and approximately 20% smaller than that obtained by Lin and Falicov (although in Ref. 7 this value of Lin and Falicov is retracted and it is claimed instead that the value is difficult to determine).

The maximum of the fifth band, designated as “H”, occurs in the mirror plane. It is labeled in Fig. S6, along with the points Γ and T, which have been included in the diagram for orientation purposes. Using a 2-D interpolation grid with a density of 5000 k-points per length of the reciprocal lattice vector, we determine the coordinates of one of these six H points to be $[0.2050, 0.3753, 0.2050]$ (fractional coordinates with respect to the reciprocal lattice vectors). The coordinates for the corresponding H point as found by Lin and Falicov are $[0.2043, 0.3758, 0.2043]$ and so the agreement is excellent. We use our point H to determine the angle

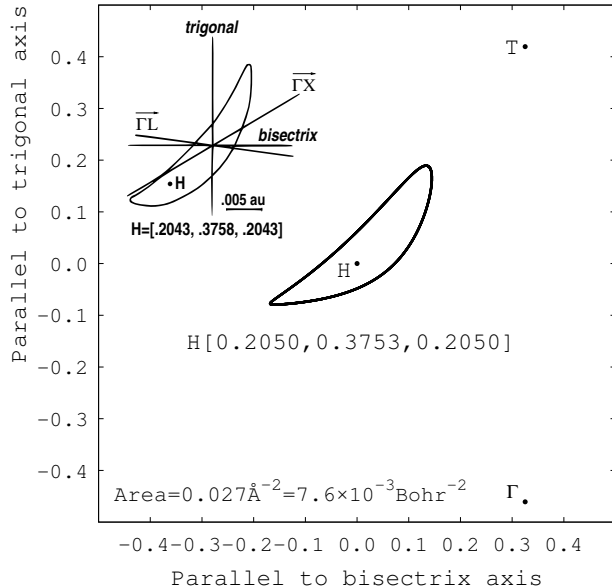


FIG. S6: Hole pocket—one of six lobes of the hole crown: trigonal-bisectrix plane through H. This figure and the resulting area have been obtained using a Fermi energy recomputed from the Wannier-interpolated DOS of A7 arsenic at 0 GPa. All distances are in \AA^{-1} . This contour can be located in the top panel of the left-hand column of Fig. 6. The inset is the analogous cross section as calculated by Lin and Falicov.¹⁴ The points Γ and T are included as an aid to viewer orientation.

that the lobe makes with the vertical to be 37.8° (this is the angle between HT and ΓT), which agrees closely with experiment.⁷

The intersection of the binary-bisectrix plane through T with the hole Fermi surface yields the contours of the cross sections of the six necks, each located about a point B along a TW line. One such cross section is depicted in Fig. S7. Again using a 2-D interpolation grid with a density of 5000 \mathbf{k} -points per length of the reciprocal lattice vector, we determine the fractional coordinates of one of these six B points to be $[0.4472, 0.4999, 0.5528]$. The coordinates for one of the B points as found by Lin and Falicov are $[0.4617, 0.5, 0.5383]$, close to our own results.

Finally, as we did with the electron Fermi surface, we look at the intersection of the trigonal-binary plane passing through Γ with the hole Fermi surface, which is illustrated in Fig. S8. We see that in this orientation, two necks are sliced vertically—they are on opposite sides of T.

Once again, all results obtained for both the electron and hole Fermi surfaces of arsenic at 0 GPa are summarized in Table I, and contrasted against results previously published in the literature. We now proceed to investigate further the evolution of the Fermi surface of arsenic with pressure.

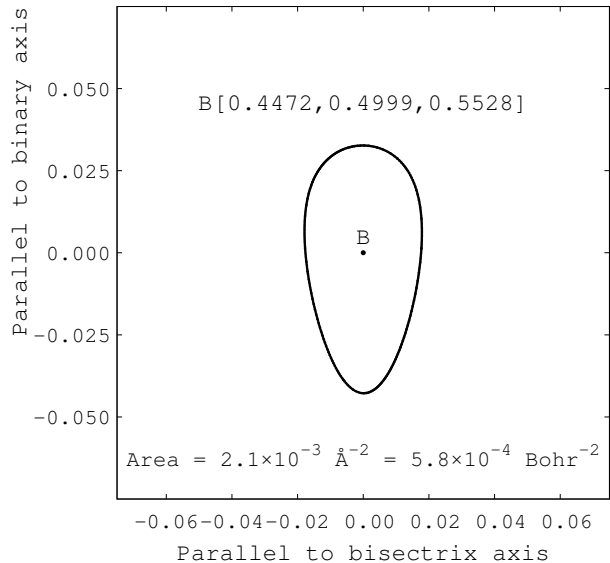


FIG. S7: Hole pocket—one of six “necks” of the hole crown: binary-bisectrix plane through T. This figure and the resulting area have been obtained using a Fermi energy recomputed from the Wannier-interpolated DOS of A7 arsenic at 0 GPa. All distances are in \AA^{-1} . This contour can be located in the top panel of the middle column of Fig. 6.

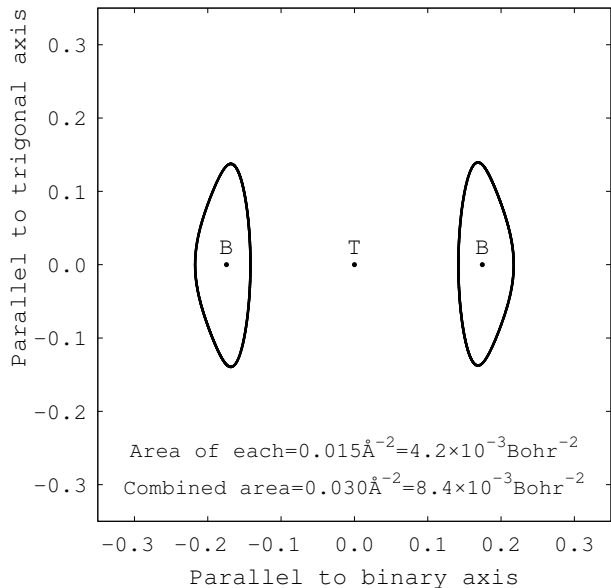


FIG. S8: Hole pocket: trigonal-binary plane through T. This figure and the resulting areas have been obtained using a Fermi energy recomputed from the Wannier-interpolated DOS of A7 arsenic at 0 GPa. All distances are in \AA^{-1} .

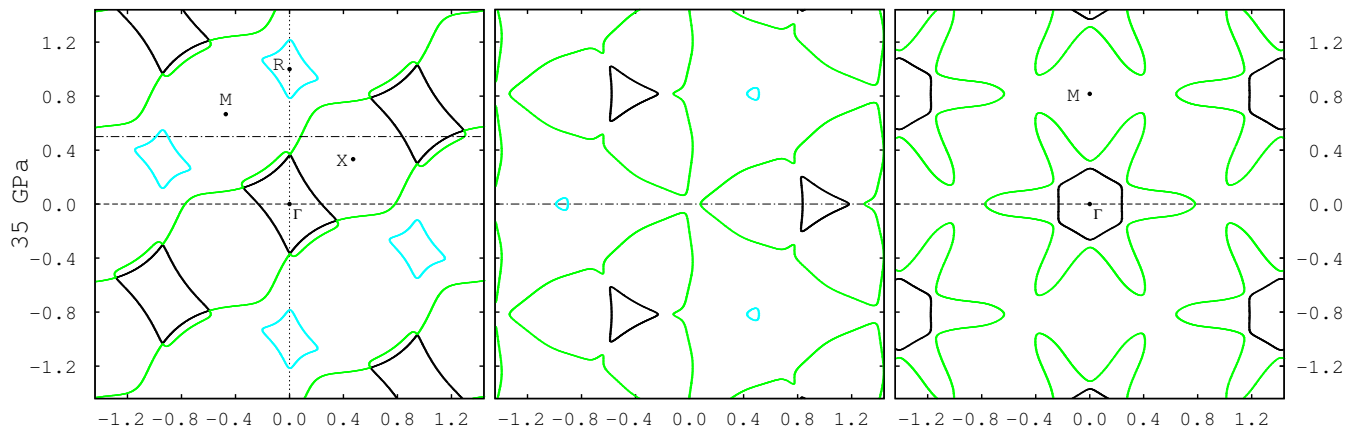


FIG. S9: This figure is the unfolded version of the bottom row of Fig. 6, obtained by slicing up the BZ of the corresponding one-atom primitive cell of sc arsenic at 35 GPa. The orientations of each of the three panels correspond to those of Fig. 6, as do the dotted, dashed and dotted-dashed lines. Distances in this figure are fractional with respect to the length of the reciprocal lattice vector of the corresponding two-atom unit cell. This is so that this figure can be overlaid and compared to the bottom row of Fig. 6. The second, third and fourth bands contribute the black, green and blue contours, respectively. In particular, the second band provides cubic hole pockets at Γ (in the left panel these are seen sliced along the body diagonal) and the fourth band provides cubic electron pockets at the points R.

SIV. PRESSURE DEPENDENCE OF THE FERMION SURFACE OF ARSENIC: A7 \rightarrow SC TRANSITION

A. SC Arsenic Using the One-Atom Primitive Cell

In Fig. S9 we display contours of the Fermi surfaces of sc arsenic at 35 GPa using the one-atom primitive cell. (The self-consistent calculation for the ground state potential of sc arsenic at 35 GPa using the one-atom primitive cell is performed using a $40 \times 40 \times 40$ Monkhorst-Pack grid of \mathbf{k} -points.) This figure is the “unfolded” version of the bottom row of Fig. 6, where the calculations have been performed for sc arsenic at 35 GPa using the two-atom unit cell. The orientation of the panels correspond between the two figures. The contours displayed in Fig. S9 are provided by bands 2 (black), 3 (green) and 4 (blue). The second band provides hole pockets at Γ , and the fourth band provides electron pockets at R. The distances in Fig. S9 are fractional with respect to the length of the reciprocal lattice vector of the two-atom unit cell of sc arsenic—this is so that the folded and unfolded versions of the figure can be overlaid and compared with each other. Points R and M that appear in the left panel of Fig. S9 fold onto the points Γ and X respectively when the two-atom unit cell is used. The origin of the middle panel of the figure is the point $[\frac{1}{4}, \frac{1}{4}, \frac{1}{4}]$, corresponding to the T point in the case of the two-atom unit cell—in order for the middle panel of this figure to correspond to the middle panel of the bottom row of Fig. 6, the plane containing the points T, W and U in the two-atom case is slid downward by the fractional coordinates $[\frac{1}{4}, \frac{1}{4}, \frac{1}{4}]$.

The top panel of Fig. S10 depicts another view of the unfolded Fermi surface of arsenic in the sc phase at 35 GPa. This slice through the one-atom sc BZ contains

Γ and the points X, and we can see the cubic hole surface centered on Γ provided by the second band. The green contours are provided by the third band. The fourth band does not cross the Fermi level for any of the \mathbf{k} -points on this slice through the sc BZ, hence the fourth band provides no contours to this slice. In order to be consistent, distances once again are with respect to the length of the reciprocal lattice vector of the two-atom unit cell.

In the bottom panel of Fig. S10, the XCrySDen package¹⁵ has been used to plot out the three-dimensional Fermi surface corresponding to the view displayed in the top panel of the figure. Surfaces due to bands 2, 3 and 4 are merged to form the object shown. The second band provides the dark green cube centered on Γ . The fourth band provides the dark blue cubes centered on R. The corresponding slice of the BZ for the two-atom representation of sc arsenic at 35 GPa is shown in Fig. S11—it is the folded version of the top panel of Fig. S10.

B. Higher-Pressure Transitions of Arsenic

Watching animations 1–3,^{16–18} we observe that arsenic ceases to be in the sc phase over 53–54 GPa, and enters the bcc phase over 95–96 GPa—there are quite dramatic changes to the Fermi contours taking place at these transition pressures. The pressures at which these transitions occur are as expected since this work is based on our earlier findings,¹⁰ as we have already mentioned. Between the sc and bcc phases, arsenic has an incommensurate structure (with increasing pressure, the progression of the phases of arsenic is A7 \rightarrow sc \rightarrow incomm \rightarrow bcc as discussed in Ref. 10). As stated in that work, we do not attempt to model properly the phase existing between sc and bcc—a periodically-repeated two-atom unit cell

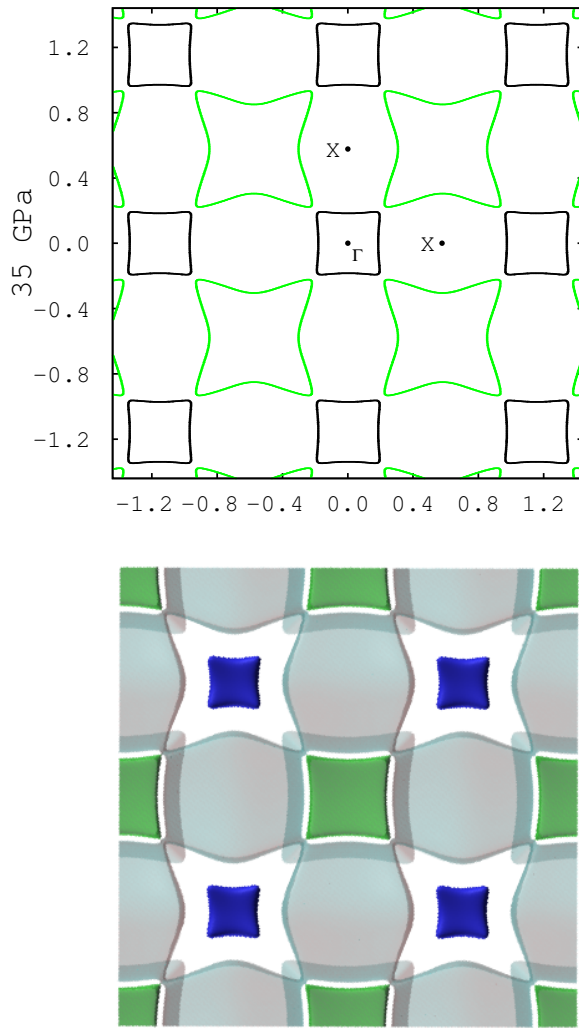


FIG. S10: Another perspective of the Fermi surface of sc arsenic at 35 GPa using the one-atom primitive cell. In the top panel, we see that for this slice through the BZ only the second and third bands provide contours (in black and green, respectively). This perspective allows us to see the actual cubic cross section of the unfolded hole pocket at Γ . Distances in the top panel are once again fractional with respect to the length of the reciprocal lattice vector of the two-atom unit cell. In the bottom panel, the 3-D Fermi surface in the direction corresponding to the slice of the top panel is plotted. The second band provides the dark green cube at Γ , the fourth band provides the dark blue cubes at the points R, and the third band provides the remainder of the object shown.

cannot model an incommensurate structure. We have acknowledged this point by simply labeling as “incomm” the structure we find between the sc and bcc phases. That being stated, in the interest of thoroughness and continuity we nevertheless use our earlier findings for this “incomm” phase (over the range of 54–95 GPa) in the same way as we have done for the other pressures studied.

At 55 GPa, arsenic is in our fictitious “incomm” phase. At 200 GPa, arsenic is in the bcc phase. In Fig. S12 we display for 55 GPa and 200 GPa the left-hand, mid-

dle and right-hand columns in the style of Fig. 6: the panels of the left-hand column refer to intersections of the trigonal-bisectrix plane with the BZ, those of the middle column to intersections of the binary-bisectrix plane through T with the BZ, and those of the right-hand column to intersections of the binary-bisectrix plane through Γ with the BZ. Once again, all distances in this figure are fractional with respect to the length of the reciprocal lattice vector. The dotted, dashed and dotted-dashed lines are as described for Fig. 6. In the two-atom representation of the bcc phase of arsenic, the points T, W and U merge. This is evinced by comparing both rows of Fig. S12: in the left-hand panels the points T and U are seen to be merged at 200 GPa, while in the middle panels this is the case for all three points. Only bands 5 (in black) and 6 (in green) are represented in this figure, though at 55 GPa bands 5–8 cross the Fermi level and at 200 GPa it is crossed by bands 3–8. For our two-atom periodically-repeated representation of arsenic at 55 GPa, bands 7 and 8 missing from the figure both provide small electron pockets at T. In the 200 GPa case, missing bands 3 and 4 give rise to very small hole pockets at X, while bands 7 and 8 produce electron pockets at T.

In a further elucidation of the might of Wannier interpolation, we conclude this section by inviting the reader to peruse some or all of the remaining animations that ac-

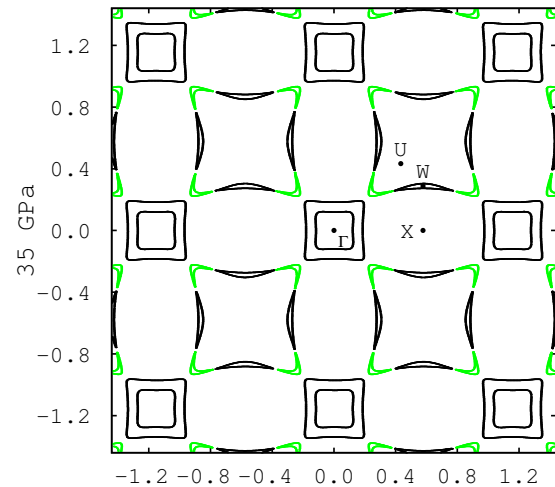


FIG. S11: Simple-cubic arsenic at 35 GPa using the two-atom unit cell: this figure is the folded version of the top panel of Fig. S10.

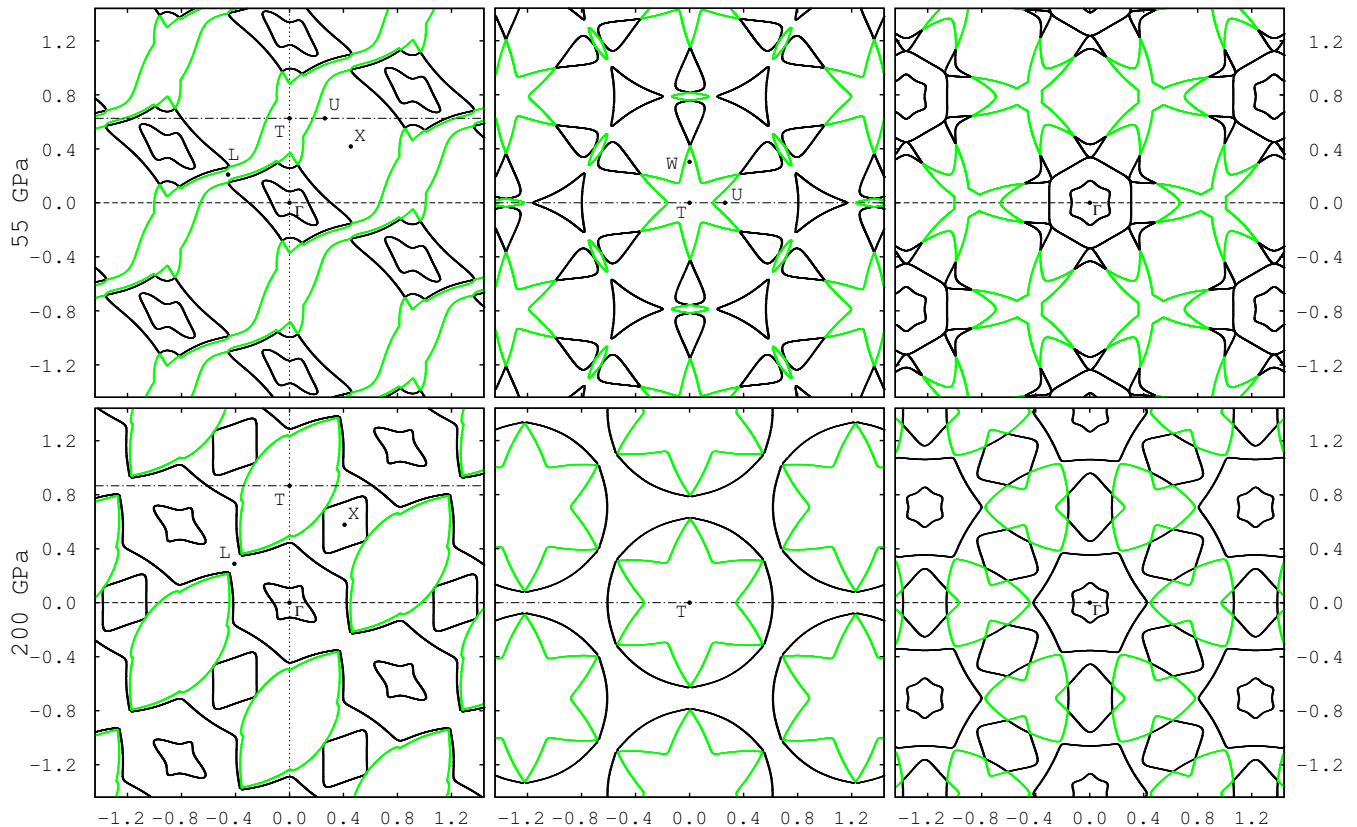


FIG. S12: Pressure dependence of the Fermi surface of arsenic: 55–200GPa. This figure is in the style of Fig. 6. The top row represents slices of the BZ for arsenic at 55 GPa, when it is in our fictitious “incomm” phase. In the bottom row we display the slices for bcc arsenic at 200 GPa.

company this work.^{19–31} Of the 16 animations that have been included, we have been discussing the three which illustrate the evolution of the Fermi surface of arsenic with pressure.^{16–18} For each of the six pressures (0, 10, 20, 35, 55 and 200 GPa) that contribute to Fig. 6 and to Fig. S12, we have plotted the two-dimensional band structure of the fifth and sixth bands corresponding to a sequence of slices through the BZ. We slice the BZ in two different directions producing two animations for each pressure:^{19–30} parallel to the trigonal-bisectrix plane and parallel to the binary-bisectrix plane. In addition to the 2-D band structures, the resulting electron and hole Fermi contours are also plotted.

Lastly, as we have also been working with the one-atom primitive cell of arsenic at 35 GPa, we have created an animation displaying the Fermi contours provided by bands 2, 3 and 4 resulting again from such slices through the BZ.³¹ The left-hand panel of each frame of this animation displays the contours arising from a slice that is parallel to a plane corresponding to the trigonal-bisectrix plane. The right-hand panel displays the contours resulting from slices parallel to a plane corresponding to the binary-bisectrix plane in the two-atom case.

SV. WANNIER-INTERPOLATED DENSITIES OF STATES OF A7, SC AND BCC ARSENIC

Finally we inspect the evolution of the DOS of arsenic in the immediate vicinity of the A7 \rightarrow sc transition, and present our results in Fig. S13. This figure consists of a series of six panels that are ordered from top to bottom, starting with the left-hand column. The top left panel displays the DOS of arsenic at 29 GPa, when it is in the sc phase. In the panels that follow, we see successive superpositions of the DOS that result as the pressure is decreased at intervals of 1 GPa. In the bottom right panel, the six DOS from 29 to 24 GPa are shown. Changes in the DOS through the sc \rightarrow A7 transition as the pressure is decreased are more clearly seen in this direction than in the reverse. We observe a marked change in the DOS between 26 and 27 GPa, as evinced by the sharp wiggles that first appear in the top right panel of the figure. These emerging van Hove singularities indicate the onset of the Peierls-type cubic to rhombohedral distortion. We reported in Ref. 10 that in the GGA-PBE case the A7 \rightarrow sc transition occurs at 28 ± 1 GPa, coinciding with the pressure at which the atomic positional parameter z reaches its high-symmetry value of $1/4$. The signature we notice in the top right panel of Fig. S13 however seems to

coincide with the change in the cell angle α (we showed in Ref. 10 that α reaches its high-symmetry value at a lower pressure than does z). In other words, the electronic change occurring as the pressure is increased appears to be driving α to 60° . Yet arsenic cannot be said to be in the sc phase until both α and z have reached their high-symmetry values. As reported in Ref. 10, for GGA-PBE the difference between these two pressures is approximately 2 GPa. The above observation does coincide however with what we see in the animations that

accompany this work.^{16–18} As we discussed in Sec. V, a folding of the Fermi surfaces is seen to occur by 27 GPa.

It is useful to be able to compare DOS plots with the band structures to which they correspond. We offer in Fig. S14 just such a comparison for the A7, sc and bcc phases of arsenic at 0, 35 and 200 GPa, respectively. In each case, the Fermi level is indicated by the solid red line. As the pressure is increased, the lowest bands begin to appear free-electron-like.

-
- ¹ G. S. Cooper and A. W. Lawson, Phys. Rev. B **4**, 3261 (1971).
- ² M. H. Cohen, Phys. Rev. **121**, 387 (1961).
- ³ M. H. Cohen, L. M. Falicov, and S. Golin, IBM J. Res. Dev. **8**, 215 (1964).
- ⁴ L. M. Falicov and S. Golin, Phys. Rev. **137**, A871 (1965).
- ⁵ L. M. Falicov and P. J. Lin, Phys. Rev. **141**, 562 (1966).
- ⁶ L. R. Windmiller, Phys. Rev. **149**, 472 (1966).
- ⁷ M. G. Priestley, L. R. Windmiller, J. B. Ketterson, and Y. Eckstein, Phys. Rev. **154**, 671 (1967).
- ⁸ C. S. Ih and D. N. Langenberg, Phys. Rev. B **1**, 1425 (1970).
- ⁹ J. P. Perdew, K. Burke, and M. Ernzerhof, Phys. Rev. Lett. **77**, 3865 (1996).
- ¹⁰ P. Silas, J. R. Yates, and P. D. Haynes, Phys. Rev. B **78**, 174101 (2008).
- ¹¹ R. M. Martin, *Electronic Structure: Basic theory and practical methods* (Cambridge University Press, 2004).
- ¹² A. A. Mostofi, J. R. Yates, Y.-S. Lee, I. Souza, D. Vanderbilt, and N. Marzari, Comput. Phys. Commun. **178**, 685 (2008), <http://www.wannier.org>.
- ¹³ I. Souza, N. Marzari, and D. Vanderbilt, Phys. Rev. B **65**, 035109 (2001).
- ¹⁴ P. J. Lin and L. M. Falicov, Phys. Rev. **142**, 441 (1966).
- ¹⁵ A. Kokalj, Comput. Mater. Sci. **28**, 155 (2003).
- ¹⁶ *Animation-1-Trigonal-bisectrix-plane-through-Gamma-with-pressure.gif*.
- ¹⁷ *Animation-2-Binary-bisectrix-plane-through-T-with-pressure.gif*.
- ¹⁸ *Animation-3-Binary-bisectrix-plane-through-Gamma-with-pressure.gif*.
- ¹⁹ *Animation-4-0GPa-parallel-to-trigonal-bisectrix-plane.gif*.
- ²⁰ *Animation-5-0GPa-parallel-to-binary-bisectrix-plane.gif*.
- ²¹ *Animation-6-10GPa-parallel-to-trigonal-bisectrix-plane.gif*.
- ²² *Animation-7-10GPa-parallel-to-binary-bisectrix-plane.gif*.
- ²³ *Animation-8-20GPa-parallel-to-trigonal-bisectrix-plane.gif*.
- ²⁴ *Animation-9-20GPa-parallel-to-binary-bisectrix-plane.gif*.
- ²⁵ *Animation-10-35GPa-parallel-to-trigonal-bisectrix-plane.gif*.
- ²⁶ *Animation-11-35GPa-parallel-to-binary-bisectrix-plane.gif*.
- ²⁷ *Animation-12-55GPa-parallel-to-trigonal-bisectrix-plane.gif*.
- ²⁸ *Animation-13-55GPa-parallel-to-binary-bisectrix-plane.gif*.
- ²⁹ *Animation-14-200GPa-parallel-to-trigonal-bisectrix-plane.gif*.
- ³⁰ *Animation-15-200GPa-parallel-to-binary-bisectrix-plane.gif*.
- ³¹ *Animation-16-35GPa-primitive-cell-showing-both-directions-simultaneously.gif*.
- ³² References in which the numbering is not preceded by an “S” refer to Figures, Sections or Tables that appear in the accompanying paper.

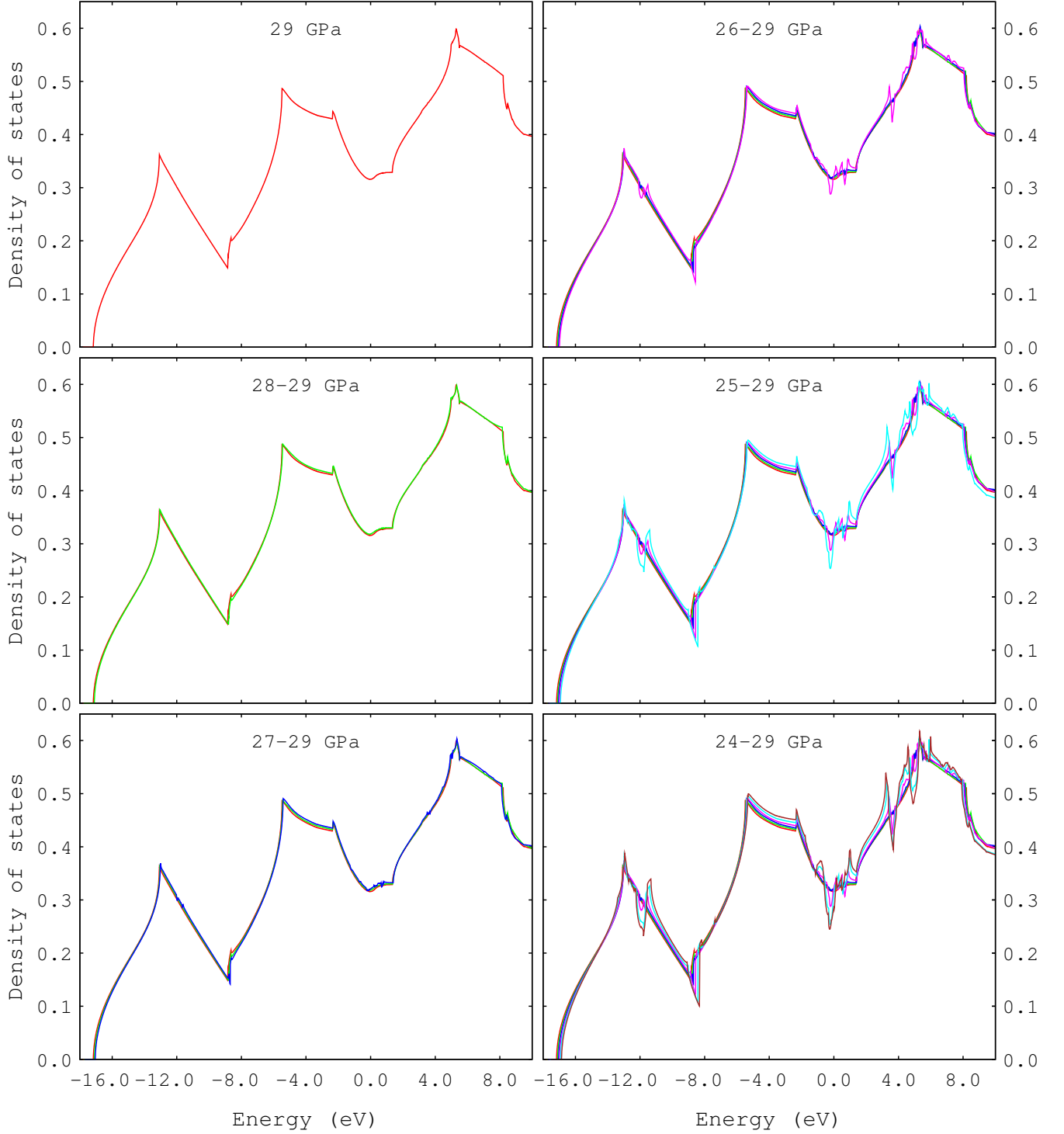


FIG. S13: Evolution of the DOS of arsenic across the $sc \rightarrow A7$ phase transition. The DOS are referenced to the Fermi level. The panels are ordered from top to bottom starting with the left-hand column. The DOS of sc arsenic at 29 GPa is presented in the top left panel. DOS at 1 GPa intervals and with decreasing pressure are added to each successive image in the panels that follow. A marked change occurs between 26 and 27 GPa, as can be seen in the top right panel. The emerging van Hove singularities indicate the onset of the Peierls-type cubic to rhombohedral distortion. This agrees with the pressure at which the perfect folding of the Fermi surfaces is seen to occur, as discussed in Sec. V and which can be observed by viewing the relevant animations.^{16–18} In Ref. 10 we reported that the electronic change that occurs across the transition drives the atomic positional parameter z to its high-symmetry value—our results here suggest instead that it is the rhombohedral angle α that is being driven to its high-symmetry value.

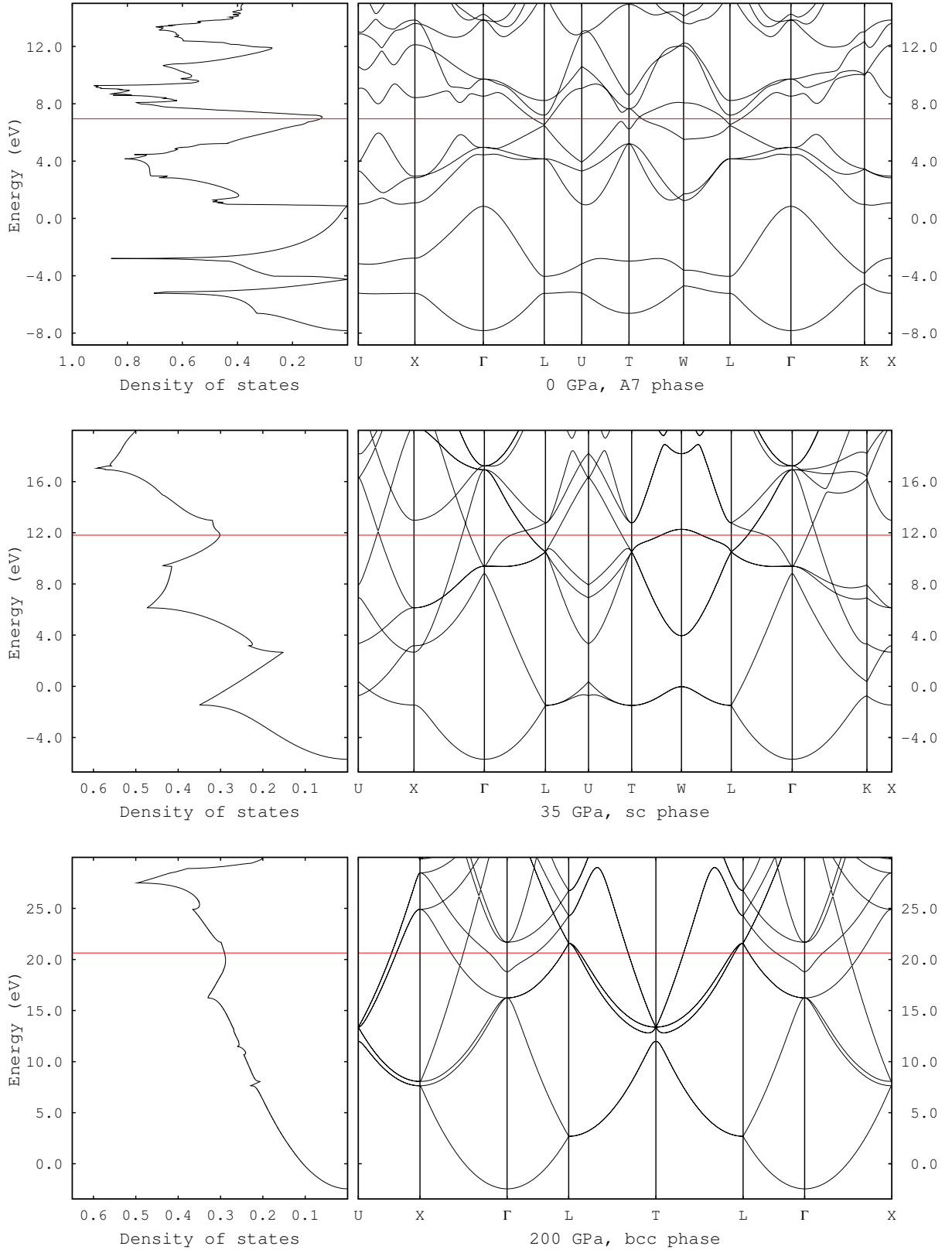


FIG. S14: The Wannier-interpolated DOS of A7, sc and bcc arsenic and corresponding band structures. In each case, the Fermi level is indicated by the solid red line. At 0 GPa, arsenic is a semimetal—from the band structure in the top panel we see that the fifth band provides tiny hole pockets at a point (called B) close to T along the TW line. The sixth band provides electron pockets at L. At 35 GPa, arsenic is a metal—the band structure displayed for sc arsenic in the middle panel is “folded”—it results from performing our calculations on a unit cell containing two atoms. Scanning the band structures from top to bottom, it can be seen that low-lying bands appear free-electron-like with increasing pressure.